ChemPubSoc Europe

DOI: 10.1002/cphc.201801042

CHEMPHYSCHEM Articles

Manipulation of Supramolecular Columnar Structures of H-Bonded Donor-Acceptor Units through Geometrical Nanoconfinement

Wongi Park[+],[a] Beatriz Feringán[+],[b] Minyong Yang,[a] Seong Ho Ryu,[a] Hyungju Ahn,[c] Tae Joo Shin,[d] Teresa Sierra,*[b] Raquel Giménez,*[b] and Dong Ki Yoon*[a, e]

Ambipolar organic semiconductors are considered promising for organic electronics because of their interesting electric properties. Many hurdles remain yet to be overcome before they can be used for practical applications, especially because their orientation is hard to control. We demonstrate a method to control the orientation of columnar structures based on a hydrogen (H)-bonded donor-acceptor complex between a star-shaped tris(triazolyl)triazine and triphenylene-containing benzoic acid, using physicochemical nanoconfinement. The molecular configuration and supramolecular columnar assemblies in a one-dimensional porous anodic aluminium oxide (AAO) film were dramatically modulated by controlling the pore-size and by chemical modification of the inner surface of the porous AAO film. In situ experiments using grazing-incidence X-ray diffraction (GIXRD) were carried out to investigate the structural evolution produced at the nanometer scale by varying physicochemical conditions. The resulting highly ordered nanostructures may open a new pathway to effectively control the alignment of liquid crystal ambipolar semiconductors.

1. Introduction

The two most important parameters of organic semiconductors in electronic devices are the high crystallinity[1–3] and orientation[4,5] of the active layer. Extensive studies have consequently investigated the relationship between charge carrier mobility and the stacking sequence of the active layer,[6,7] which is commonly known as the π-orbital overlap phenomena. Pentacene, whose aromatic moieties are used as the active layer, is a representative material for studying this relationship.[8,9] However, the lack of tools to control the fine orientation of pentacene molecules hinders the use of this ideal semiconductor material in practical organic electronics. To solve the orientation problem, studies have focused on aromatics containing molecules with aliphatic spacer groups, to induce segregated self-assembly in columnar structures,[10,11] where disc-like molecules that have aromatic moieties and alkyl tails are closely stacked together. These structures exhibit high charge carrier mobility along the columnar axis. Previous studies dealing with discotic molecules have shown that, usually, either electrons or holes are transported,[10] although both electron and hole transport layers are required for the p-n junction, which is essential for organic electronics.[11,12]

As a result, it has been necessary to develop ambipolar organic semiconductors that can transport both electrons and holes simultaneously. In a recent study[13] on the use of columnar liquid crystals in organic electronics, some donor-acceptor complexes showed good properties for both electron and hole mobility by using a combined supramolecular/columnar liquid crystal approach; specifically, donor-acceptor supramolecules formed by H-bonding a star-shaped tris(triazolyl)triazine acceptor to three triphenylene-derived donors.[13] In that work, the orientation of the columnar structures could not be controlled in a large area because of the lack of long range order,[14] although there are reported some successes with columnar structures of common discotic liquid crystals. To control the orientation of ambipolar discotic molecules,[15–19] conventional alignment methods such as surface treatment,[20–22] mechanical shearing,[23–25] and rubbed polymer layer[26,27] cannot uniaxially guide the columnar structures. To solve this problem, nanoconfinement[28–32] has emerged as a powerful tool, and is useful to generate well-oriented supramolecular structures in various kinds of organic materials. Porous anodic aluminum oxide (AAO) nanochannels[33] are used

[a] W. Park,[+] M. Yang, S. H. Ryu, Prof. Dr. D. K. Yoon
Graduate School of Nanoscience and Technology
Korea Advanced Institute of Science and Technology (KAIST)
Daejeon 34141, Republic of Korea
E-mail: nandk@kaist.ac.kr
[b] Dr. B. Feringán,[+] Dr. T. Sierra, Dr. R. Giménez
Departamento de Química Orgánica
Instituto de Ciencia de Materiales de Aragón (ICMA)
Facultad de Ciencias, Universidad de Zaragoza-CSIC
Zaragoza, 50009 Spain
E-mail: tsierra@unizar.es
rgimenez@unizar.es
[c] Dr. H. Ahn
Pohang Accelerator Laboratory
POSTECH
Pohang, 37673, Republic of Korea
[d] Prof. Dr. T. J. Shin
UNIST Central Research Facilities
and School of Natural Science
UNIST, Ulsan, 44919, Republic of Korea
[e] Prof. Dr. D. K. Yoon
Department of Chemistry and KINC
Korea Advanced Institute of Science and Technology (KAIST)
Daejeon, 34141, Republic of Korea
[+] These authors contributed equally to this work

Supporting information for this article is available on the WWW under https://doi.org/10.1002/cphc.201801042

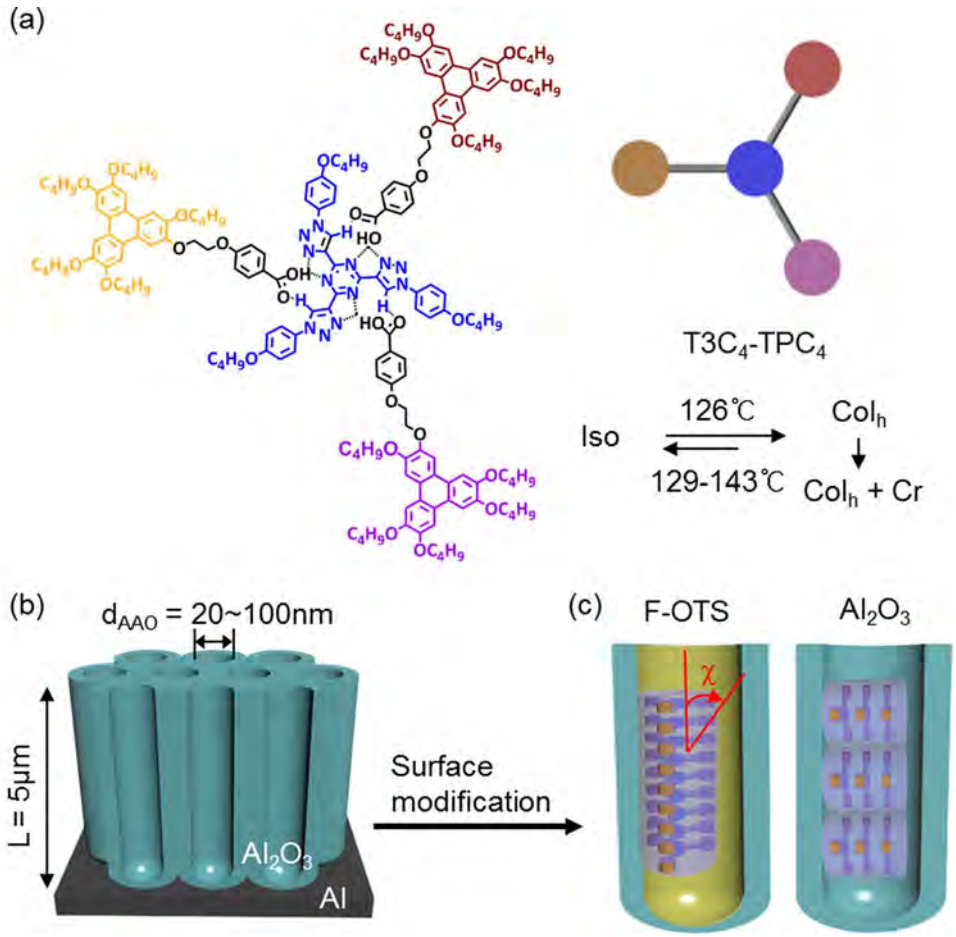

Figure 1. Schematic illustration of ambipolar discotic molecules and AAO nanochannels. a) Molecular structure and thermal phase transition of $T3C_4$–TPC_4. b) Schematic illustration of porous AAO nanochannels and different molecular alignments inside the channel depending on the surface conditions with c) FOTS and aluminum oxide.

to maximize the surface anchoring effect on the molecules because these confined geometries can have a very high surface/volume ratio. In addition, a surface modification can be used to modify the surface energy of the inner surface of the nanochannel, providing an additional effort to control the orientation of the organic molecules.

In the present work, we employ the physicochemical nanoconfinement approach using AAO nanochannels and surface modification to obtain uniaxially oriented columns made of a hydrogen (H)-bonded donor-acceptor complex. Grazing incidence X-ray diffraction (GIXRD) experiments with synchrotron radiation were performed to directly investigate the orientation and configuration of the assembled columnar structures under different conditions at the molecular level. The resulting highly aligned columns in the nanochannel might be used as "modules" to fabricate organic electronics, such as organic field effect transistors and solar cells, in the near future.

2. Results and Discussion

To implement our strategy, the supramolecular complex $T3C_4$–TPC_4 was prepared by dissolving the tris(triazolyl)triazine core and the triphenylene-containing benzoic acid in a 1:3 ratio in dichloromethane (Figure 1a). The mixture was evaporated to dryness, dried under vacuum and subjected to a thermal treatment consisting of heating at 155 °C and fast cooling to room temperature. Formation of the H-bonded complex was confirmed by FTIR, and was in agreement with previously reported complexes (Figure S1 in the Supporting Information).[13,34] The brown, red, and purple discs are all the same moieties or molecules, but are represented in different colors to show their detailed molecular configuration with varying physicochemical conditions (Figure 1a). By using polarized optical microscopy (POM), differential scanning calorimetry (DSC) (Figure S2) and powder X-ray diffraction (XRD) analysis, it was confirmed that the fast-cooled complex arranges in a hexagonal columnar mesophase, Col_h at room temperature, with a lattice parameter of $a = 37.3$ Å. A diffuse halo in the wide angle region around 4.5 Å corroborated the liquid crystal nature of the phase, and a relatively sharp reflection at 3.4 Å indicated

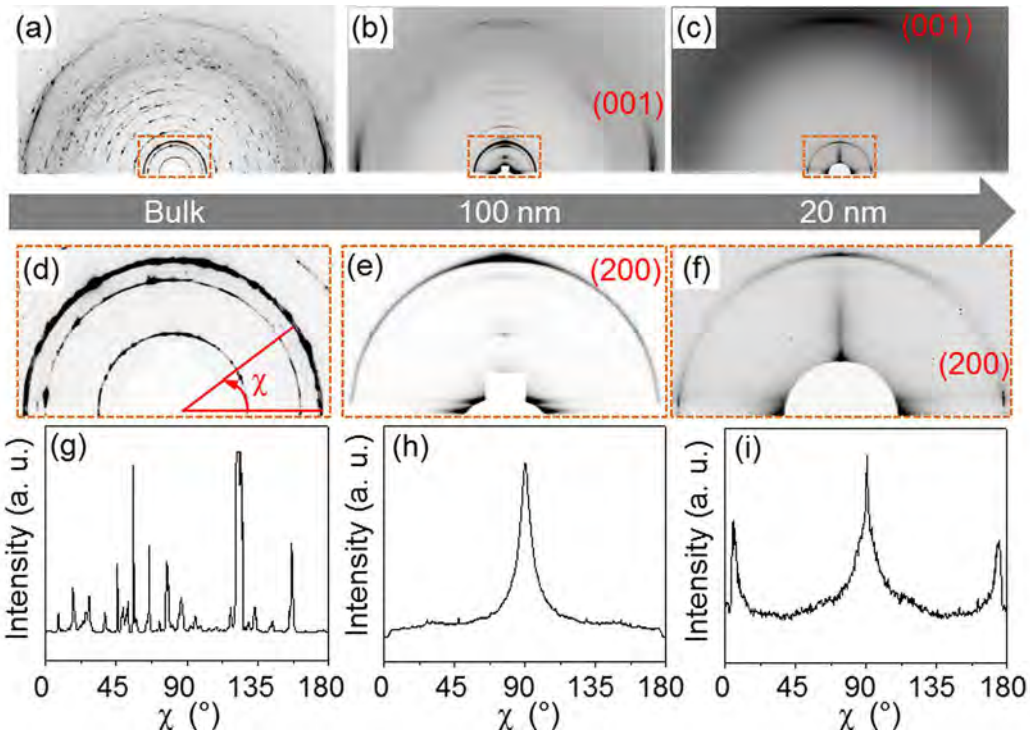

Figure 2. GIXRD results for $T3C_4$–TPC_4 depending on the various physicochemical confinement conditions. Two-dimensional GIXRD patterns of $T3C_4$–TPC_4 placed on a) a flat aluminium oxide substrate, and in nanochannels with different pore diameters of $d_{AAO} = 100$ nm (b) and $d_{AAO} = 20$ nm (c). Enlarged GIXRD patterns showing the (200) planes of $T3C_4$–TPC_4 for various substrate conditions: d) on bulk, e) in a $d_{AAO} = 100$ nm nanochannel, and f) in a $d_{AAO} = 20$ nm nanochannel, and their 1D circular cut graphs (g–i) in the (200) lattice, respectively.

intracolumnar order (Figure S3, Table S1). The observed reflections are consistent with a highly ordered columnar arrangement with $T3C_4$–TPC_4 as the stacking unit. The phase is not thermodynamically stable and the bulk sample tends to crystallize if the sample is slowly cooled from the isotropic liquid. This is clearly observed in the diffractogram by the appearance of sharp reflections in the wide angle region (Figure S4). Therefore, this is a case where, in bulk, the Col_h phase is a metastable phase observed on supercooling.

For the nanoconfinement, a porous AAO nanochannel was synthesized as previously reported.[21,35] Oxalic and sulfuric acids were used with an applied electric field to form ~100 nm- and ~20 nm-pores, respectively, in high-purity annealed aluminum foil (Figure S5). The depth of the channel (L) used in this experiment was fixed at 5 μm, and the pore diameters (d_{AAO}) were 20 nm and 100 nm (Figure 1b). The resultant nanochannel was composed of aluminum oxide, and offered high surface energy for organic molecules to induce planar anchoring.[21] In general, the orientation of small molecular weight discotic molecules on the substrate is governed by the chemical affinity between the surface and molecule.

To change the orientation of the $T3C_4$–TPC_4 molecules and the corresponding columnar structures, the inner surface of the nanochannel was modified with a material that can induce the molecules to perpendicularly align to the substrate; here, tridecafluoro-1,1,2,2-tetrahydrooctyltrichlorosilane (FOTS) was used.[21] As a result, the molecules arranged differently, as shown in Figure 1c. To perform the experiment, three kinds of distinctive experimental conditions were prepared. The first compared the effects of physical nanoconfinement in the columnar structures of varying pore sizes; 20 nm and 100 nm pore pristine AAO nanochannels were used (Figure 2). The second involved chemical varied-affinity experiments, comparing an aluminium oxide/FOTS-surface with $T3C_4$–TPC_4 in the 100 nm-nanochannel (Figure 3). The third was a physicochemical treatment combining the two conditions mentioned above, using the FOTS-treated 20 nm and 100 nm pore-nanochannels (Figure 5).

The physicochemical nanoconfinement sample preparation method employs a simple to use capillary to infiltrate $T3C_4$–TPC_4 in the isotropic phase, ~140 °C, then after carefully removing the residuals on top of the channel with fabrics, which selectively removed the complex molecules outside the pores of AAO films, the sample is cooled to room temperature, ~20 °C at a slow rate of 0.2 °C min^{-1}. This maximizes the surface anchoring effect by providing enough time for the molecules to align in a given condition. Since the heating stage is placed under the sample, a cooling thermal gradient is generated in the nanochannel. Temperature is the lowest at the top of the nanochannel because the sample is open to air. The nucleation of the columnar structure begins at the isotropic to Col_h phase transition temperature. This sort of gradient cooling helps to minimize nucleation sites in the nanochannels, leading to the sequential growth of columnar structures along the channel

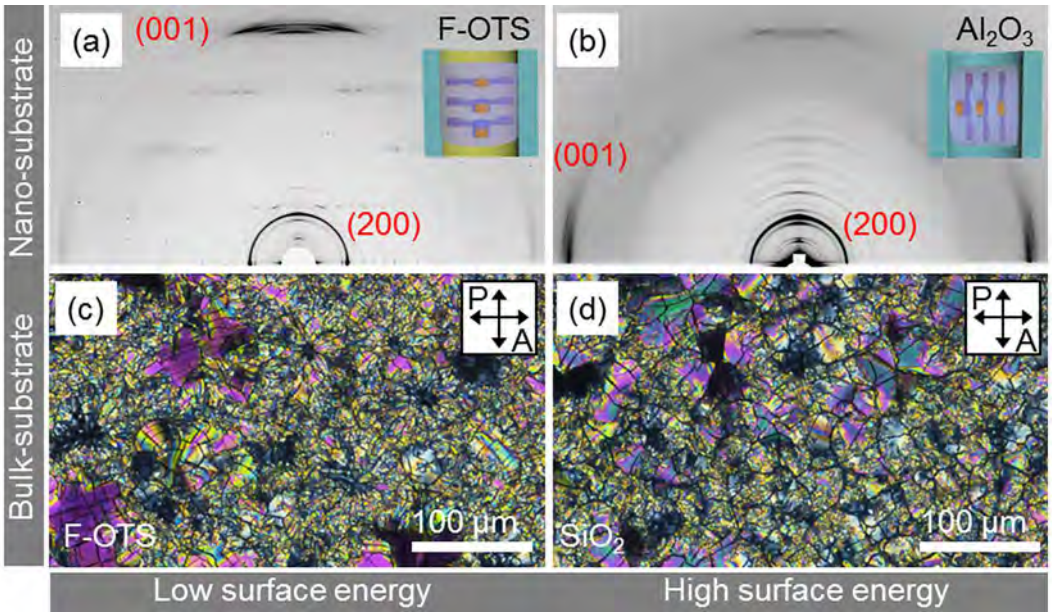

Figure 3. Structural analysis of $T3C_4$–TPC_4 based on chemical affinity-varied interactions in 100 nm pore-AAO nanochannels, and on a bulk substrate. Two-dimensional GIXRD results depending on the surface energy of the AAO nanochannel (d_{AAO} = 100 nm) with a) FOTS and b) aluminum oxide. Polarized optical microscope images in sandwich cells which have different surface conditions with c) FOTS and d) SiO_2.

direction, or radial/perpendicular to the inner surface of the nanochannels, depending on surface energy conditions (Figure 1c).

Grazing-incidence X-ray diffraction (GIXRD) experiments using a synchrotron radiation source were performed to analyze the columnar structures in bulk and under nanoconfinement conditions (Figure 2 and Figure S6). In our experiment, the orientation of the columns and molecular configuration were the two most important factors, thus a two-dimensional (2D) CCD camera was used as a detector, to give both in-plane and out-of-plane information of the aligned columnar structures. Quite different GIXRD patterns were obtained (Figure 2) by varying the physical nanoconfinement conditions in the bulk state, 100 nm- and 20 nm-nanochannels, and showed a clear tendency as the physical confinement conditions changed. Here, each surface was pristine condition aluminium oxide, so we expected that most of the molecules would be arranged parallel to the aluminium oxide surface.

Here, two important XRD peaks, (200) in the small angle region and (001) in the wide angle region, are mainly discussed because they provide information about the inter-columnar and intra-columnar assembly behavior, respectively.[31] In the bulk state, a powder sample was simply dropped on the substrate, heated up to the isotropic phase and cooled to room temperature. The resultant 2D GIXRD results show typical polycrystalline-like diffraction patterns that have no specific orientation (Figure 2a, 2d, 2 g). In the 100 nm-nanochannel sample, sharp (001) peaks at $\chi \sim 0^\circ$ and 180° in the wide angle region are observed (Figure 2b), while a strong (200) peak at $\chi \sim 90^\circ$ is observed in the small angle region (Figure 2e, 2 h). This indicates the $T3C_4$–TPC_4 molecules and the corresponding columnar structures are mostly-aligned in the nanochannel. Here, the (200) peaks is unusually strong compared with (100) peaks, which is similar to the XRD result in the previous study,[13] in which the (200) reflection may receive the additional contribution of planes containing triphenylene moieties.

Interestingly, totally different patterns were obtained from the sample confined in the 20 nm-nanochannel, where a relatively large arc (001) peak was observed at $\chi \sim 90^\circ$ in the wide angle region (Figure 2c), while three sharp peaks appeared at $\chi \sim 0^\circ$, 90°, and 180° at the (200) position with a little variation in intensity (Figure 2f, 2i). Based on these results, one can observe that nanostructures with different orientations are formed as the geometrical scale decreases from bulk to 20 nm. The orientation of the stacks of the aromatic core and the columns can be inferred from the position of the (001) and (200) peaks, which are related to intra-columnar and inter-columnar scattering, respectively. In the bulk, no specific orientation is observed in the (001) and (200) lattice which means a lack of orientation in the macroscale. In contrast, the specific alignment of molecules in the nanochannel can be confirmed by the (001) and (200) peaks. In the 100 nm-nanochannel, discotic molecules are aligned parallel to the inner surface of the channel with face-on orientation and the corresponding columns are aligned vertically; this could reflect either a log pile configuration[32] or radial configuration.[36] However, in the 20 nm-nanochannel, most of the stacks of aromatic cores are aligned perpendicularly to the surface and the columns are axially oriented, even though there are some possible escaped-radial morphology which can be inferred by the peak at 90° in the (200) reflection. It seems that the stronger curvature of the 20 nm pore prevents the growth of the perpendicularly oriented columns, as reported previously.[31,37,38]

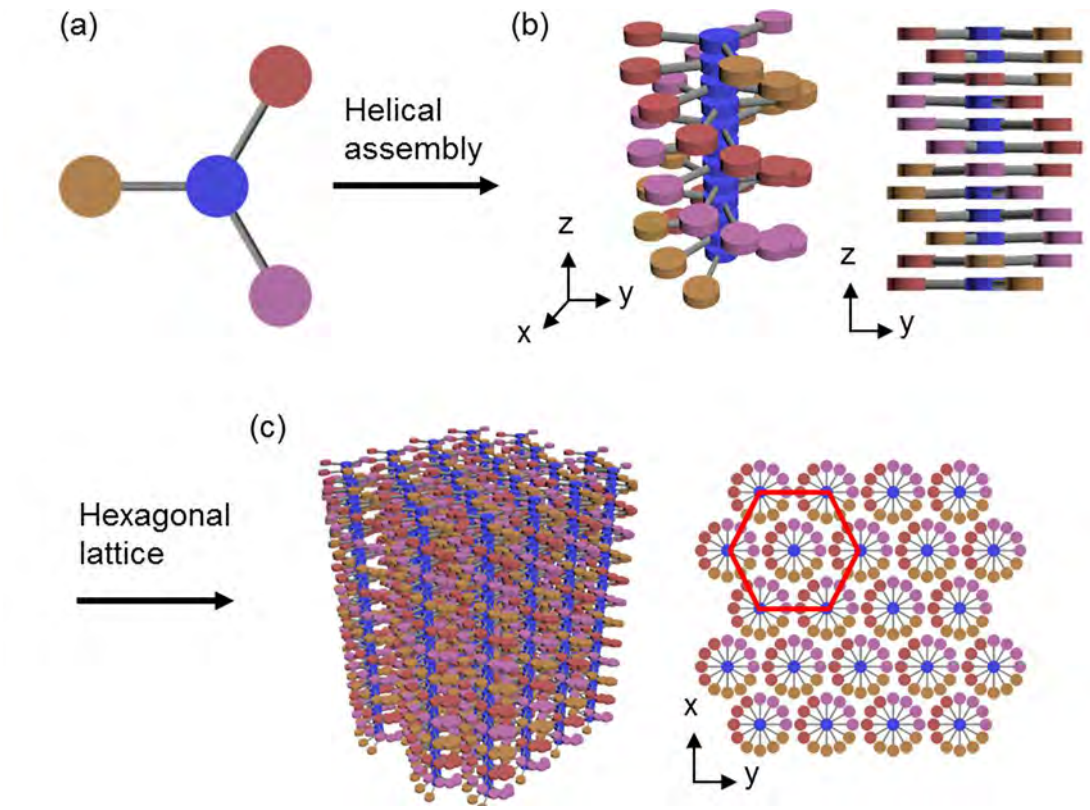

Figure 4. Sketch of a columnar structure model inside the FOTS treated 100 nm-AAO nanochannel. a) Molecular structure of $T3C_4$–TPC_4 with 3-fold symmetry. Schematic illustration of b) a single column that is made of helically assembled molecules and c) bundles of columns which have hierarchically assembled into an in-plane hexagonal lattice.

The GIXRD patterns of the supramolecular structures in the 100 nm pore-AAO nanochannels with different surface anchoring conditions in aluminium oxide and FOTS are shown in Figure 3a and 3b, indicating the structural changes that occur with varying chemical affinities. Totally different GIXRD patterns can be observed in the two samples: In the FOTS condition, strong (001) peaks are observed at $\chi \sim 90^\circ$, which means that the stacks of the aromatic cores are aligned parallel to the axis of the nanochannel. However, in the aluminium oxide condition, the same peaks are oriented at $\chi \sim 0^\circ$ and 180°, which indicates perpendicularly aligned aromatic cores. In order to fully understand the orientation of the columnar structure, extra GIXRD experiments were performed with $T3C_4$–TPC_4 in the FOTS-treated 100 nm pore-nanochannel upon heating (Figure S7). Because the peak positions of the (200) plane are distributed at $\chi \sim 0^\circ$, 90° and 180° (Figure S7a and S7d), it is difficult to define the orientation of the columns in the nanochannel at low temperature. But, as the temperature rises, the GIXRD patterns show clearer orientational directions in the small angle region (Figure S7). Since the strong (200) peaks only occurred at $\chi \sim 0^\circ$ and 180°, the columns are oriented axially in the AAO nanochannel. Probably, thermal treatment caused the partial melting of minor radial structure and clearly makes the axially oriented peak. This helped us to conclude that the final structure is based on the major axial orientation with minor radial orientation. All of those patterns disappeared in the isotropic phase (Figure S7c). From these results, it was confirmed that the diffraction patterns originated with the $T3C_4$–TPC_4 molecules, and the nanostructures are basically aligned uniaxially with small distortion at room temperature with small portion of radial orientation.

This phenomenon is unusual in bulk environments where molecules are located between glass substrates under different surface conditions (Figure 3c, 3d). Like the case mentioned above, two types of different surface conditions were used, $FOTS/SiO_2$. In the bulk substrate, due to the low surface/volume ratio, the $Cr(Col_h)$ domain was not successfully controlled, although it was already reported that those two conditions in the bulk state offer different surface anchors to general organic molecules. This result in the bulk substrate clearly demonstrates the effectiveness of the nanoconfinement system for manipulating supramolecular structures. Figure 4 shows how $T3C_4$–TPC_4 is self-assembled in the FOTS-treated 100 nm pore-nanochannel based on the confirmation of the molecular and columnar orientation. Four parallel patterns marked in Figure S7b indicate a helical assembly, which has been already demonstrated.[39] The four parallel lines, which are perpendicular to the axis of the columns in Figure S7b, suggest a 4_1 helical columnar structure. As the $T3C_4$–TPC_4 molecule itself has 3-fold symmetry (Figure 4a), the supramolecular structure forms a 12_3 helical columnar configuration (Figure 4b) and the rotation angle between the adjacent molecules is around 30°. These helical

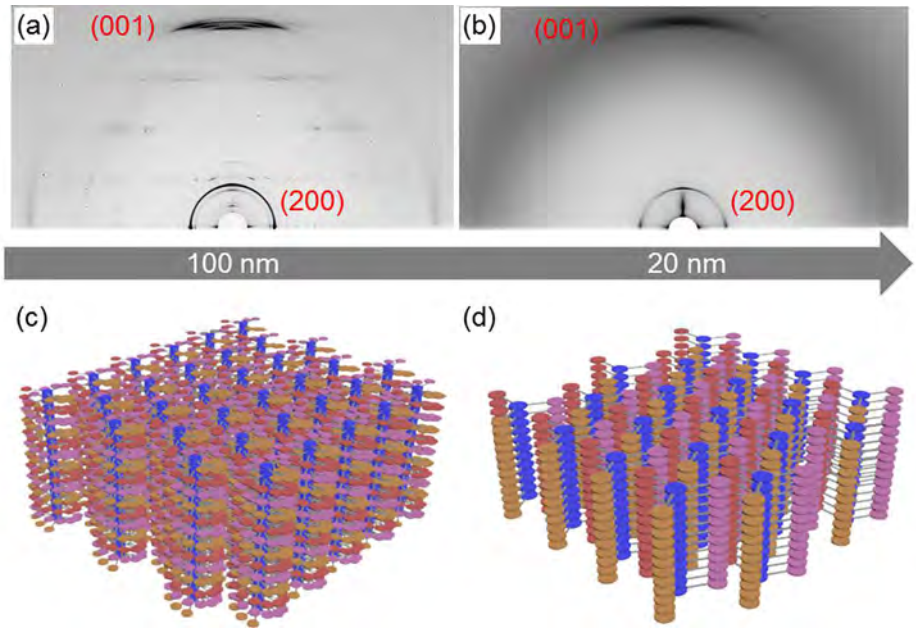

Figure 5. Structural modification under tight geometrical condition (in FOTS condition). 2D image of GIXRD under FOTS condition but in different D_p: a) 100 nm and b) 20 nm. The tighter geometrical condition suppresses the helical structure and exhibits a much simpler diffraction pattern (b). Each diffraction can be explained by a helical columnar hexagonal structure (c) and (d) a coaxial columnar hexagonal structure (d).

columns hierarchically assemble together and eventually form the in-plane hexagonal packing, as shown in Figure 4c. The diffraction patterns in Figure 3a and 3b can also be explained precisely by this helical columnar structure. Once again, in the FOTS-treated 100 nm pore-nanochannel (Figure 3a and 5a), the crystal structure forms helical columnar structures which are uniaxially aligned in the channel. In comparison to this, in the aluminium oxide nanochannel, the molecules form the same helical columns but are aligned perpendicularly to the channel, which can be explained by either log pile configuration or radial configuration. Both of the log pile and radial configurations have already been reported previously.[32,36,40,41] Due to the topological frustration arising from the restricted geometry, the inside core part orientations were suggested either of axial or isotropic state. In Figure 3b, there is no (200) diffraction in $\chi \sim 0°$, 180° which indicates the isotropic core orientation.[36] In other words, by changing the chemical affinity between the surface and molecule, the stacking direction of the aromatic cores, which is related to the electrical properties, can be controlled.[42] This is well matched with the previous studies about discotic liquid crystal molecules in nanochannels. The face-on orientation of the discs which was caused by the aluminum oxide induced the radial configurations of the columns[40] and the edge-on orientation by the FOTS surface made the axial configurations of columns.[38,40] Although the donor-acceptor complex forms the helical columnar structure, same phenomenon has been observed. From this result, it is reconfirmed that the molecular anchoring on the surface of the template is the main reason for the columnar orientations in nanochannel.

More interestingly, another diffraction pattern appeared in the 20 nm pore-channel (Figure 5b). In conditions tighter than the 100 nm pore-channel, it seems that the crystal phase is suppressed, and the sample has the typical diffraction pattern of the liquid crystal phase (Col_h).[31] Regardless of the surface treatment, the $T3C_4$–TPC_4 molecules make the same diffraction pattern (Figure 2c and 5b). The (001) diffraction in the wide angle region is observed at $\chi \sim 90°$ without any parallel line pattern in the middle angle region, which is observed in the 100 nm pore (Figure 5a). This resulting pattern indicates a simple columnar structure without any helix, with the columns uniaxially oriented in the nanochannel (Figure 5d).

A direct comparison of the self-assembled structures in the 100 nm and 20 nm pores, which were both treated by FOTS, is summarized in Figure 5. In the larger pore environment, the molecules tend to crystallize and form a helical columnar structure (Figure 5c). However, in the tighter geometrically confined system, the crystallization is suppressed, and normal columns are generated, just like the columnar liquid crystal phase (Figure 5d). This might be explained by the previously reported results showing the suppression of highly ordered structure in tighter geometrical nanoconfinement.[43] For similar reason, the highly ordered helical columnar structure was suppressed because of the geometrical restriction.

3. Conclusions

In summary, we successfully controlled the orientation of a donor–acceptor supramolecular columnar liquid crystal. Columnar liquid crystal structures in porous nano-templates have

been studied steadily since the last decade.[31,36–38,44,45] It has been revealed that the various surface modification and the size of the porous structures can control the orientations of the columnar structures; radial, face-on log pile, circular concentric, axial and etc. Hence, the highly ordered columnar nanostructure can be suppressed due to the restricted geometry. Based on these theoretical and experimental foundations, ambipolar discotic liquid crystals can be successfully controlled and investigated. As the size of the substrates which confine the organic materials decreased, the increased surface/volume ratio of the template enhanced the surface anchoring condition and successfully controlled the orientation and configuration of the organic molecules, which have previously been difficult to control. Furthermore, the low surface energy condition provided by the FOTS induces a uniaxial orientation in the columns, forming a distinct GIXRD pattern. The structure was determined to be a helical columnar hexagonal structure. Previously, because of the lack of uniaxial alignment, detailed molecular configurations such as the helical assembly were not observed. This AAO nanochannel based organic/inorganic composite with ambipolar charge transport property can not only be useful as an approach for internal visualization, but can also be used as a "module" to fabricate advanced organic electronics like vertical field effect transistors and solar cells.

Experimental Section

Materials and Methods

$T3C_4$–TPC_4 was prepared from the precursors 2,4,6-tris[1-(4-butoxyphenyl)-1,2,3-triazol-4-yl]-1,3,5-triazine and 4-[2-(3,6,7,10,11-pentabutyloxytriphenylen-2-oxy)ethoxy]benzoic acid, that were synthesized by adapting previously described procedures.[13,34] NMR spectra were acquired on a Bruker AV400 spectrometer and referenced using the solvent residual peak. Infrared spectra were recorded on a Nicolet Avatar 380 spectrometer with KBr pellets. DSC thermograms were acquired with a TA instruments Q-20 apparatus at a rate of 10 °C min^{-1}. Powder X-ray experiments of bulk samples were performed in a Pinhole diffractometer (Anton Paar) operating with a point focused Ni-filtered Cu–Kα beam. The sample was hold in a Lindemann glass capillary (0.9 mm diameter). The diffraction patterns were collected on photographic film.

Synthesis of $T3C_4$–TPC_4

To prepare the supramolecular complex, a mixture of 2,4,6-tris[1-(4-butoxyphenyl)-1,2,3-triazol-4-yl]-1,3,5-triazine (0.049 mmol, 35.8 mg) and 4-[2-(3,6,7,10,11-pentabutyloxytriphenylen-2-oxy) ethoxy]benzoic acid (0.148 mmol, 113.9 mg) were dissolved in dry dichloromethane (20 mL). The solution was stirred to dryness in an orbital shaker (240 rpm) at room temperature. Once the solvent was evaporated, the mixture was introduced into a vacuum desiccator at 40 °C for 24 hours. Finally, a thermal treatment was performed, which consisted of heating the mixture at 155 °C with a fast cool down to room temperature. ^{1}H NMR (400 MHz, CD_2Cl_2) δ 9.01 (s, 3H), 8.09–8.07 (m, 6H), 7.96 (s, 3H), 7.840–7.77 (m, 21H, ArH), 7.09–7.07 (m, 12H), 4.65–4.57 (m, 6H), 4.57–4.47 (m, 6H), 4.29–4.14 (m, 30H), 4.05 (t, J = 6.5 Hz, 6H), 1.96–1.78 (m, 36H), 1.65–1.49 (m, 36H), 1.09–0.98 (m, 54H). ^{13}C NMR (100 MHz, CD_2Cl_2) δ 170.7, 167.3, 163.8, 160.5, 149.8, 149.7, 149.7, 149.6, 148.7, 146.3, 132.8, 130.3, 124.9, 123.8, 123.8, 122.8, 115.9, 115.0, 109.7, 107.7, 107.5, 107.4, 107.4, 107.3, 69.8, 69.7, 69.7, 69.2, 68.8, 67.9, 32.1, 32.0. 31.8, 19.9, 19.8, 14.3, 14.2. FTIR (KBr, cm^{-1}): 1708 (C=O st).

Preparation of Nanochannels

High-purity annealed aluminium foil (Alfa Aesar) was rinsed with acetone, ethanol and deionized water. The aluminium foil was then electrochemically polished in a solution which contained perchloric acid and ethanol at 20 V. Depending on the target diameter of the nanochannel pore, either oxalic acid (100 nm) or sulfuric acid (20 nm) were used as an anodizing electrolyte. The final pore diameter (D_P) was determined by chemical etching process, called pore widening, in a phosphoric acid solution. To give them a different surface anchoring condition, tri-deca-fluoro-1,1,2,2-tetrahydrooctyl-trichlorosilane (FOTS) was coated on the inner surface of the channel. The AAO nanochannels were initially treated by O_2 plasma for 10 min to give them hydroxyl groups for subsequent silanization. The FOTS molecules were deposited onto the substrate via vapor deposition method under vacuum condition for 1 h. After removing the excess FOTS molecules, thermal annealing was performed at 120 °C for complete chemisorption between the substrate and FOTS.

Imaging the Optical Textures in Sandwich Cells

The sandwich cells were made with two glass substrates which were rinsed with acetone, ethanol, and DI water. Silica particle spacers were used to maintain a 3 μm distance between the cell substrates. Polarized optical microscopy (POM) (LV100POL, Nikon, Tokyo, Japan) was used to examine the birefringence textures of the organic materials.

Grazing Incidence X-ray Diffraction

The $T3C_4$–TPC_4 complex was infiltrated into the AAO nanochannel (10×10 mm^2 area that is much bigger than the X-ray beam spot size of 70 μm (vertical) by 300 μm (horizotal) via capillary force. The grazing incidence X-ray diffraction (GIXRD) experiments were performed at the 9 A U-SAXS and 6D C&S UNIST-PAL beamlines of Pohang Accelerator Laboratory (PAL). The focused energy of the beam source was 11.06 keV and the sample-to-detector distance (SDD) was set to be around 323 mm to observe the intercolumnar and intracolumnar orientation simultaneously. The diffraction patterns were recorded with a 2D CCD camera (Rayonix SX165).

Author Contributions

W.P. and B.F. contributed equally to this work. W.P., B.F., T.S., R.G. and D.K.Y. designed the research; B.F., T.S. and R.G. synthesized and made initial characterization of the discotic molecule; W.P. and S. H. R. synthesized the AAO; W.P., M.Y., H.A. and T.J.S. performed GIXRD experiments; W.P., B.F., T.S., R.G. and D.K.Y analyzed results and wrote the manuscript.

Acknowledgements

This study was supported by a grant from the National Re-search Foundation (NRF) and funded by the Korean Government (2017M3C1A3013923 and 2017R1E1A1A01072798), the Spanish

Government MINECO-FEDER funds (project MAT2015-66208-C3-1-P), and the Gobierno de Aragón-FSE (research group E47-17R and B.F. grant B084/13). The experiments at the PLS-II were supported in part by MSIT and POSTECH.

Conflict of Interest

The authors declare no conflict of interest.

Keywords: self-assembly · supramolecular column · anodic aluminium oxide · confinement

[1] A. A. Virkar, S. Mannsfeld, Z. Bao, N. Stingelin, *Adv. Mater.* **2010**, *22*, 3857–3875.
[2] D. J. Gundlach, J. E. Royer, S. K. Park, S. Subramanian, O. D. Jurchescu, B. H. Hamadani, A. J. Moad, R. J. Kline, L. C. Teague, O. Kirillov, C. A. Richter, J. G. Kushmerick, L. J. Richter, S. R. Parkin, T. N. Jackson, J. E. Anthony, *Nat. Mater.* **2008**, *7*, 216–221.
[3] X. Ye, Y. Liu, Q. Han, C. Ge, S. Cui, L. Zhang, X. Zheng, G. Liu, J. Liu, D. Liu, X. Tao, *Chem. Mater.* **2018**, *30*, 412–420.
[4] A. L. Briseno, J. Aizenberg, Y.-J. Han, R. A. Penkala, H. Moon, A. J. Lovinger, C. Kloc, Z. Bao, *J. Am. Chem. Soc.* **2005**, *127*, 12164–12165.
[5] T. Matsukawa, S.-I. Kobayashi, T. Onodera, H. Oikawa, K. Itaya, *Mater. Chem. Phys.* **2013**, *137*, 947–950.
[6] I. O. Shklyarevskiy, P. Jonkheijm, N. Stutzmann, D. Wasserberg, H. J. Wondergem, P. C. M. Christianen, A. P. H. J. Schenning, D. M. d. Leeuw, ž. Tomović, K. Müllen, J. C. Mann, *J. Am. Chem. Soc.* **2005**, *127*, 16233–16237.
[7] D. T. James, B. K. C. Kjellander, W. T. T. Smal, G. H. Gelinck, C. Combe, I. McCulloch, R. Wilson, J. H. Burroughes, D. D. C. Bradley, J.-S. Kim, *ACS Nano*, **2011**, 5, 9824–9835.
[8] S. K. Park, T. N. Jackson, J. E. Anthony. D. A. Mourey, *Appl. Phys. Lett.* **2007**, *91*, 063514.
[9] Y. Diao, B. C. Tee, G. Giri, J. Xu, D. H. Kim, H. A. Becerril, R. M. Stoltenberg, T. H. Lee, G. Xue, S. C. B. Mannsfeld, Z. Bao, *Nat. Mater.* **2013**, *12*, 665–671.
[10] T. Wöhrle, I. Wurzbach, J. Kirres, A. Kostidou, N. Kapernaum, J. Litterscheidt, J. C. Haenle, P. Staffeld, A. Baro, F. Giesselmann, S. Laschat, *Chem. Rev.* **2016**, *116*, 1139–1241.
[11] S. Laschat, A. Baro, N. Steinke, F. Giesselmann, C. Hägele, G. Scalia, Ro. Judele, E. Kapatsina, S. Sauer, A. Schreivogel, M. Tosoni, *Angew. Chem. Int. Ed.* **2007**, *46*, 4832–4887; *Angew. Chem.* **2007**, *119*, 4916–4973.
[12] O. Thiebaut, H. Bock, E. Grelet, *J. Am. Chem. Soc.* **2010**, *132*, 6886–6887.
[13] B. Feringán, P. Romero, J. L. Serrano, C. L. Folcia, J. Etxebarria, J. Ortega, R. Termine, A. Golemme, R. Giménez, T. Sierra, *J. Am. Chem. Soc.* **2016**, *138*, 12511–12518.
[14] S. H. Ryu, D. K. Yoon, *ACS Appl. Mater. Interfaces.* **2016**, *8*, 17707–17712.
[15] K. Hatsusaka, K. Ohta, I. Yamamoto, H. Shirai, *J. Mater. Chem.* **2001**, *11*, 423–433.
[16] W. Pisula, Ž. Tomović, B. E. Hamaoui, M. D. Watson, T. Pakula, K. Müllen, *Adv. Funct. Mater.* **2005**, *15*, 893–904.
[17] T. Kajitani, Y. Suna, A. Kosaka, T. Osawa, S. Fujikawa, M. Takata, T. Fukushima, T. Aida, *J. Am. Chem. Soc.* **2013**, *135*, 14564–14567.
[18] A. Tracz, J. K. Jescka, M. D. Watson, W. Pisula, K. Müllen, T. Pakula, *J. Am. Chem. Soc.* **2003**, *125*, 1682–1683.
[19] C. –Y. Liu, A. J. Bard, *Chem. Mater.* **2000**, *12*, 2353–2362.
[20] H. Kim, S. Lee, T. J. Shin, Y. J. Cha, E. Korblova, D. M. Walba, N. A. Clark, S. B. Lee, D. K. Yoon, *Soft Matter.* **2013**, *9*, 6185–6191.
[21] S. H. Ryu, H. Ahn, T. J. Shin, D. K. Yoon, *Liq. Cryst.* **2016**, *44*, 713–721.
[22] W. Zheng, C. –Y. Chiang, I. Underwood, *Mol. Cryst. Liq. Cryst.* **2011**, *540*, 94–101.
[23] Y. J. Cha, M. –J. Gim, H. Ahn, T. J. Shin, J. Jeong, D. K. Yoon, *ACS Appl. Mater. Interfaces.* **2017**, *9*, 18355–18361.
[24] Y. J. Cha, D. K. Yoon, *Adv. Mater.* **2017**, *29*, 1604247.
[25] J. Kim, N. Yamasaki, T. Hayashi, H. Yoshida, H. Moritake, A. Fujii, Y. Shimizu, M. Ozaki, *Appl. Phys. Express.* **2013**, *6*, 061702.
[26] S. H. Ryu, M. –J. Gim, Y. J. Cha, T. J. Shin, H. Ahn, D. K. Yoon, *Soft Matter.* **2015**, *11*, 8584–8589.
[27] R. You, D. A. Paterson, J. M. D. Storey, C. T. Imrie, D. K. Yoon, *Liq. Cryst.* **2017**, *44*, 168–176.
[28] H. Kim, S. Lee, T. J. Shin, E. Korblova, D. M. Walba, N. A. Clark, S. B. Lee, D. K. Yoon, *Proc. Natl. Acad. Sci. USA* **2014**, *111*, 14342–14347.
[29] H. Kim, A. Zep, S. H. Ryu, H. Ahn, T. J. Shin, S. B. Lee, D. Pociecha, E. Gorecka, D. K. Yoon, *Soft Matter.* **2016**, *12*, 3326–3330.
[30] S. Lee, H. Kim, T. J. Shin, E. Tsai, J. M. Richardson, E. Korblova, D. M. Walba, N. A. Clark, S. B. Lee, D. K. Yoon, *Soft Matter.* **2015**, *11*, 3653–3659.
[31] H. Duran, B. Hartmann-Azanza, M. Steinhart, D. Gehrig, F. Laquai, X. Feng, K. Müllen, H.-J. Butt, G. Floudas, *ACS Nano.* **2012**, *6*, 9359–9365.
[32] R.-B. Zhang, G. Ungar, X. Zeng, Z. Shen, *Soft Matter.* **2017**, *13*, 4122–4131.
[33] W. Lee, S.-J. Park, *Chem. Rev.* **2014**, *114*, 7487–7556.
[34] B. Feringán, P. Romero, J. L. Serrano, R. Giménez, T. Sierra, *Chem. Eur. J.* **2015**, *21*, 8859–8866.
[35] H. Kim, S. H. Ryu, M. Tuchband, T. J. Shin, E. Korblova, D. M. Walba, N. A. Clark, D. K. Yoon, *Sci. Adv.* **2017**, *3*, e1602102.
[36] C. V. Cerclier, M. Ndao, R. Busselez, R. Refort, E. Grelet, P. Huber, A. V. Kityk, L. Noirez, A. Schönhals, D. Morineau, *J. Phys. Chem. C.* **2012**, *116*, 18990–18998.
[37] M. Steinhart, S. Zimmermann, P. Göring, A. K. Schaper, U. Gösele, C. Weder, J. H. Wendorff, *Nano Lett.* **2005**, *5*, 429–434.
[38] R. Zhang, X. Zeng, B. Kim, R. J. Bushby, K. Shin, P. J. Baker, V. Percec, P. Leowanawat, G. Ungar, *ACS Nano,* **2015**, *9*, 1759–1766.
[39] C. Roche, H.-J. Sun, M. E. Prendergast, P. Leowanawat, B. E. Partridge, P. A. Heiney, F. Araoka, R. Graf, H. W. Spiess, X. Zeng, G. Ungar, V. Percec, *J. Am. Chem. Soc.* **2014**, *136*, 7169–7185.
[40] A. V. Kityk, M. Busch, D. Rau, S. Calus, C. V. Cerclier, R. Lefort, D. Morineau, E. Grelet, C. Krause, A. Schönhals, B. Frick, P. Huber, *Soft Matter,* **2014**, *10*, 4522–4534.
[41] S. Calus, A. V. Kityk, P. Huber, *Microporous Mesoporous Mater.* **2014**, *197*, 26–32.
[42] D. Khim, A. Luzio, G. E. Bonacchini, G. Pace, M.-J. Lee, Y.-Y. Noh, M. Caironi, *Adv. Mater.* **2018**, *30*, 1705463.
[43] R. J. Bushby, O. R. Lozman, *Curr. Opin. Colloid Interface Sci.* **2002**, *7*, 343–354.
[44] J. Kopitzke, J. H. Wendorff, *Liq. Cryst.* **2000**, *27*, 643–648.
[45] K. Sentker, A. W. Zantop, M. Lippmann, T. Hofmann, O. H. Seeck, A. V. Kityk, A. Yildirim, A. Schönhals, M. G. Mazza, P. Huber, *Phy. Rev. Lett.* **2018**, *120*, 067801.

Manuscript received: November 8, 2018
Revised manuscript received: December 23, 2018
Accepted manuscript online: February 7, 2019
Version of record online: February 27, 2019